

Soft Matter

Accepted Manuscript



This is an *Accepted Manuscript*, which has been through the Royal Society of Chemistry peer review process and has been accepted for publication.

Accepted Manuscripts are published online shortly after acceptance, before technical editing, formatting and proof reading. Using this free service, authors can make their results available to the community, in citable form, before we publish the edited article. We will replace this *Accepted Manuscript* with the edited and formatted *Advance Article* as soon as it is available.

You can find more information about *Accepted Manuscripts* in the [Information for Authors](#).

Please note that technical editing may introduce minor changes to the text and/or graphics, which may alter content. The journal's standard [Terms & Conditions](#) and the [Ethical guidelines](#) still apply. In no event shall the Royal Society of Chemistry be held responsible for any errors or omissions in this *Accepted Manuscript* or any consequences arising from the use of any information it contains.

ARTICLE

Physico-chemical Confinement of Helical Nanofilaments

Cite this: DOI: 10.1039/x0xx00000x

S. Lee^{a†}, H. Kim^{a†}, T. J. Shin^b, E. Tsai^c, J. M. Richardson^d, E. Korblova^d, D. M. Walba^d, N. A. Clark^e, S. B. Lee^{a,f*} and D. K. Yoon^{a*}Received 00th January 2012,
Accepted 00th January 2012

DOI: 10.1039/x0xx00000x

www.rsc.org/

The helical nanofilaments (HNFs) have attracted much interest because of their unique optical properties, but there have been many hurdles to use these for the practical applications due to the structural complexity. Here we demonstrate that the molecular configuration and layer conformation of modulated HNF (HNFs_(mod)) can be studied using physicochemical confinement system. The layer directions affected by the chemical affinity between the mesogen and surface were drastically controlled in surface-modified nanochannels. Furthermore, an *in-situ* experiment using grazing-incidence X-ray diffraction (GIXD) was carried out to investigate in detail the structural evolution through thermal transitions. The results demonstrate that the HNF_(mod) structure can be perfectly controlled for functional HNF device applications, and a combined system with chemical and physical confinement effects will be helpful for better understanding of the fundamentals of soft matter.

Introduction

Bent-core liquid-crystal (LC) phases have been of interest to researchers because of their chiral structures. These structures have exotic physicochemical properties, which originate from spontaneously broken symmetries even though the LC material itself does not have any chiral centre such as a chiral carbon¹⁻³. A strong nanosegregation of bent-core molecules can result in macroscopic polar, chiral, or in some cases, modulated layered structures³⁻⁶, forming a variety of ferroelectric or anti-ferroelectric phases that are useful for opto-electronic applications such as non-linear optics⁷⁻⁹.

Among the layered structures of bent-core LC phases, the B4 (helical nanofilament, HNF) phase is the most complex structure, in which⁵⁻⁷ layers are helically twisted, with specific dimensions of ~35 nm in diameter and ~110 nm in half-pitch^{3,10-11}. Owing to the symmetry breaking of sublayers of the bent-core molecule, deformation of the local saddle-splay layer occurs simultaneously in the flat layered structures. For example, the fluid B2 smectic phase, which is the higher-temperature phase, can be formed, and the deformed layers are simultaneously cleaved to form HNFs⁵. Recently, modulated HNFs (HNFs_(mod)) have been reported¹². They are quite different from the normal or classic HNFs, exhibiting an in-layer modulation that has been shown to be in the B1 phase

(columnar structures) or the B7 phase (polarisation- and splay-modulated layers). However, the origin of this modulation cannot be satisfactorily explained because of its structural complexity and uncontrollability. Complete understanding of these modulations is of critical importance in order to provide the structural control needed for the practical applications mentioned above.

In this study, we observed the dramatic conformational change of HNFs_(mod) compared to classic HNF in nanoconfinement using a porous anodic aluminium-oxide (AAO) film, in which the inner surfaces of pores were chemically modified via surface sol-gel methods¹³⁻¹⁵. Here, nanoconfinement was used to form individually controlled, isolated HNFs to minimise the complexity of HNFs¹⁶, a strategy that has previously been used to control the orientation of nanostructures of various soft matters¹⁷⁻¹⁹. Moreover, chemical treatment to manipulate the aversion or affinity to LC molecules is also important in controlling the initial orientation of bent-core molecules during the thermal phase transition from isotropic to B phases.

Results and discussion

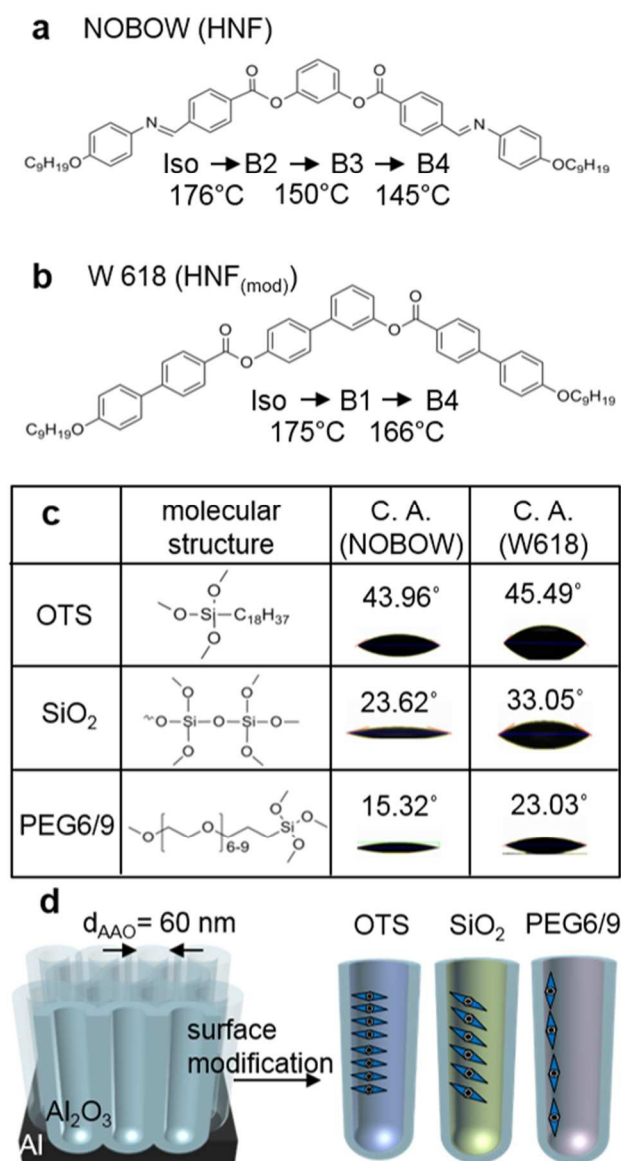


Figure 1. Liquid-crystal molecules and experimental scheme. Thermal phase transitions of a, NOBOW and b, W618. Two bent-core molecules were loaded into AAO nanochannels modified with SAMs of c, OTS, SiO₂, and PEG 6/9. To analyze the interactions between the SAMs and LC molecules, contact-angle measurements were performed at the isotropic-phase temperature of both molecules, revealing high and low contact angles depending on the LC-molecule-philic or LC-molecule-phobic properties. d, Chemically modified nanoconfinement was prepared in AAO nanochannels measuring 60 nm in diameter and 5 μm in length. Based on the contact-angle measurements, the orientation of bent-core molecules on the chemical modified nanochannel could be controlled.

To implement this strategy, two bent-core LC materials were prepared: 1,3-phenylenebis[4-(4-octoxyphenylimino ethyl) benzoate] (NOBOW) with the HNF phase and biphenyl-3,4'-diyl bis-(4'-alkoxybiphenyl-4-carboxylate) (W618) with the HNF_(mod) phase at room temperature, with different thermal phase transitions (Fig. 1a, b). Upon cooling of NOBOW in the

isotropic phase, the B2 phase, which is a polar and chiral layer structure (Fig. S1 in Supplementary Materials), appeared⁵. The tilted NOBOW molecules were then horizontally packed to form in-plane stacked layers that were locally splayed in saddle-like shapes. Finally, HNFs were formed. The B1 phase, which first appeared upon cooling of W618 in the isotropic phase, has a discrete rectangular columnar unit cell composed of parallel aligned molecules. As the B1 phase transitioned to the B4 phase, a change from the rectangular columnar structure to a smectic layered phase occurred, which can be explained by molecules in the column sliding to form a pseudo-smectic layer²⁰, after which the deformation of a similar layer led to the formation of HNFs_(mod).

Basically, the B4 phases formed by NOBOW and W618 looked very similar under normal conditions, but they were highly responsive to perturbations, which resulted in very different saddle-splay structures because of different higher-temperature phases for each molecule. Here, a simple surface treatment using various self-assembled monolayers (SAMs) was used to induce the perturbation. Previous results showed that this simple method could control the global orientation of HNFs, in which the polar direction of HNFs composed of NOBOW molecules (Fig. 1a) were precisely controlled depending on their chemical affinity to the modified surface²¹. In order to explore the relationship between the surface energy and HNF structure, we designed porous AAO films modified with various SAMs, using three kinds of organofunctional alkoxy silane molecules, octadecyltrimethoxysilane (OTS), silica, and 2[(methoxy (polyethylenoxy) propyl) trimethoxysilane (PEG 6/9) (Fig. 1c), to vary the surface energy.

To investigate the molecular interaction between a LC droplet and various SAMs, silicon wafers modified with SAMs were used for contact-angle measurements. Since the energy of the LC-air interface, γ_{LG} , was unknown, it was difficult to determine a simple calculated value of the energy of the solid-substrate-LC interface, γ_{SL} . Therefore, only the contact angles measured at the isotropic-phase temperature (180 °C) could be compared to the chemically modified surface-LC interfacial energy, γ_{SL} , showing the relative values of affinity between each LC and the modified surface. Droplets of both NOBOW and W618 had the highest contact angles on the OTS-modified surface that exhibited relatively low γ_{SL} . On the SiO₂- and PEG 6/9-modified surfaces, the respective contact angles gradually decreased, showing high γ_{SL} at the isotropic-phase temperature (Fig. 1 c). The results of the contact-angle measurements reflect the bulk properties in the isotropic phase, which also determined the global orientation of the LC layer with respect to the modified substrate and was indicative of what would happen on the inner surfaces of the porous AAO film.

The preparation of controlled HNFs in a porous AAO film was previously reported, in which the helical pitch, width, and shape of the HNFs could be varied by adjusting the nanochannel diameter in the AAO film from 20 to 80 nm¹⁶. A fixed channel diameter such as 60 nm was used here (Fig. 1d). After silanization of the inner surfaces of the AAO nanochannels via a surface sol-gel process, activated silanol sites on the AAO surfaces were modified with the organosilane SAMs. The sample was then loaded from the top of the porous AAO film at high temperature as its isotropic phase, and it was then cooled down to form the B4 phase. A heating stage was placed under the AAO film to produce a thermal gradient from the bottom to the top of the sample in order to induce the

directional, thermal phase transition. In this configuration, the thermal phase transition proceeded from the top point of the sample as the temperature decreased. During this process, the molecular orientations in the B2 and B1 phases were determined; the molecules were aligned parallel to the LC-molecule-philic (high surface energy) surface such as the PEG 6/9-treated substrate, while perpendicularly aligned molecules were found on the LC molecule-phobic (low surface energy) surface such as the OTS-treated substrate. This orientation in the higher-temperature phase governed the direction of the bulk HNFs as previously reported²¹, in which the long axis of the

materials and surface chemical properties (Fig. 2). A typical B4 structure of NOBOW in an untreated AAO nanochannel has been analysed before¹⁴, and it can be regarded as a reference for the other samples under different circumstances. NOBOW in the nanochannel displayed similar HNF structures in OTS-, SiO₂-, and PEG 6/9-modified surfaces (Fig. 2a–c); however, the dimensions of the structure, such as the helical half pitch (*hp*), thickness of the exposed layer surface (*d_{LS}*), and angle with the long axis (Ψ), were changed in accordance with the surface interaction.

In particular, HNFs in the PEG 6/9-treated nanochannels were flattened compared to other cases. For example, *d_{LS}* was 40% greater for the surface treated with PEG 6/9 than that for the surface treated with OTS; the Ψ also increased from 30° to 41°. Since the strong interaction between the PEG 6/9-treated surface and NOBOW molecules could reduce the elastic energy of the intrinsic curvature of the layers in HNFs¹⁰, more molecules were attracted to the inner surfaces of the nanochannels than in the other cases, thus resulting in flattened HNFs. This surface-anchoring interaction in the case of NOBOW was not strong enough to hinder the formation of the helical structure because the transition from B2 phase to B4 phase was relatively smooth and could endure this perturbation. On the other hand, W618 in PEG 6/9-modified nanochannels generated deformed, bamboo-like structures because of the strong interaction between W618 and the PEG 6/9-modified surface, although the B4 phase of W618 still showed general helical shapes in OTS- and SiO₂-treated nanochannels (Fig. 2d–f). This was a result of the unstable structural transition from discrete columnar domains in the B1 phase to layered structures in the B4 phase. Therefore, B1 domains remained in a bamboo-like structure that had undulated disk-like layers, shown as thin disks (*d_{LS}* ~ 26 nm) with saddle-splay curvature in the scanning electron microscope (SEM) images in Fig. 2f. Details of the half-pitch and layer thickness distribution of HNFs and HNFs_(mod) in various modified nanochannels are shown in Fig. S2.

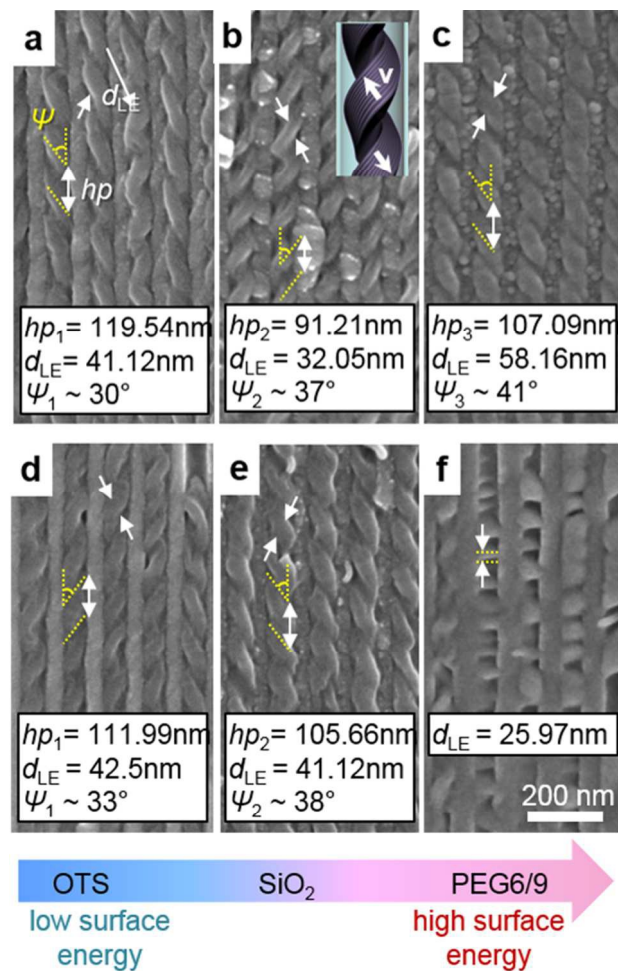


Figure 2 Cross-sectional SEM images of HNFs in various chemically modified AAO nanochannels. HNFs of NOBOW molecules were formed on a, OTS-, b, SiO₂-, and c, PEG 6/9-coated surfaces. Even though the thickness of the exposed layer surface (*d_{LS}*) was slightly increased in c, the stability of the helical structure was maintained. W618 confined on the d, OTS- and e, SiO₂-coated surfaces also showed the HNF structure, but on the f, PEG 6/9-coated surface, the morphologies were deformed to bamboo-like structures.

HNFs was aligned with the layer-parallel vector of the B2/B1 layered structure.

Combining physical and chemical confinement

The confined B4 structures in the surface-modified nanochannels could be divided into two types, depending on the

Internal nanostructure variation

In order to fully understand this dramatic change in the SEM images, grazing-incidence X-ray diffraction (GIXD) experiments with a synchrotron radiation source were carried out using samples of W618 prepared in OTS-, SiO₂-, and PEG 6/9-coated AAO nanochannels at room temperature (Fig. 3). Because of the regular arrangement of HNFs in the nanochannels, the 2-dimensional (2D) diffraction patterns showed well-oriented and very sharp peaks even though the X-ray beam size (~500 μm in diameter) was bigger than the HNFs. In the resulting 2D diffraction patterns, the azimuthal angle, χ , was defined in the range from 0° at the *q_z* axis to 90° at the *q_r* axis, as shown in Fig. 3a, representing the tilted angle of layers of HNFs. In the OTS-treated LC-molecule-phobic SAM nanochannels, diagonal patterns were clearly observed, corresponding to the structure shown in earlier studies; the other peak appeared at χ ~ 0° (Fig. 3b)^{3,16}. As reported for bulk HNFs_(mod) of W618, there were two main peaks: one indicates layer spacing ($q_1 = 0.136 \text{ \AA}^{-1}$, $d_1 = 46.2 \text{ \AA}$) and the other indicates in-layer modulation ($q_2 = 0.158 \text{ \AA}^{-1}$, $d_2 = 39.8 \text{ \AA}$)¹². Based on the findings of this study, the in-layer modulation is believed to have resulted from the change in structural periodicity by rotation of the polar direction in molecules. Based on the earlier study on bulk HNFs_(mod), we could easily

estimate the values of q_1 (0.148 \AA^{-1}) at $\chi = 60^\circ$ and weak q_2 (0.157 \AA^{-1}) at $\chi = 0^\circ$ for W618 in OTS-modified AAO. These peaks can be clearly seen in a 1D-line cut graph in Fig. 3c.

stacked in a discrete cylindrical cage or unit cell with the same polar direction, and bunches of cylinders with different polar direction are also positioned alternately with a certain distance

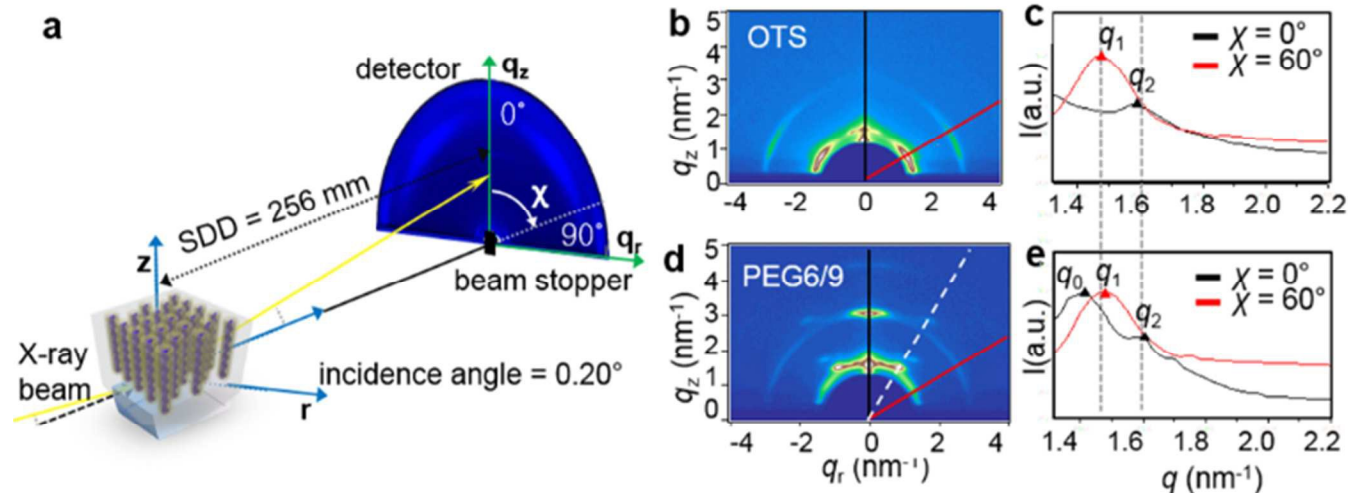


Figure 3 GIXD studies of W618 layered structures confined in surface-modified nanochannels. a, Schematic diagram of GIXD measurement. The X-ray beam was passed through the sample, and the azimuthal angle χ is defined in the range from the q_z axis to the q_r (x - y plane) axis in 2D patterns. b, 2D GIXD patterns of W618 HNFs_(mod) in OTS-coated nanochannels show typical diagonal peaks representing interlayer structures. c, 1D line-cut graph shows layer (q_1) at $\chi = 60^\circ$ and in-layer modulation (q_2) at $\chi = 0^\circ$. d, W618 in PEG 6/9 coated nanochannels exhibited a strong peak near the q_z axis and layer undulation peaks (white dashed line); its e, 1D line-cut graph.

In the case of PEG 6/9-coated AAO, the layer peaks of deformed bamboo-like structures are shown in the GIXD patterns (Fig. 3d, e), in which the most notable result compared to the OTS-coated AAO was a totally different orientation of layers. In the 2D diffraction pattern, the layer peak was now on the line along with $\chi \sim 0^\circ$, corresponding to the aligned smectic layers parallel to the bottom of the nanochannels, as observed in the SEM image in Fig. 2f. In the 1D line-cut graph, q_1 (0.142 \AA^{-1}) at $\chi \sim 0^\circ$ and elongated peaks along the same q_r axis were found, with a similar value for q_z , which resulted from the modulated layered structure. This can be explained by the strong interaction between the W618 molecules and the PEG 6/9 surface. Thus, W618 molecules could be adjoined to the inner surface of the AAO nanochannel in the very first stage just under the isotropic phase more strongly than in the case of the OTS-modified AAO. This resulted in a quenched layered structure all the way to the B4 phase at room temperature. In particular, closely packed columns in the B1 phase slide to form the deformed layer structures because they had a slightly different q value during the thermal phase transition²⁰. However, this was a competition between intrinsic saddle-splay deformation and surface anchoring, and these two interactions could be comparable. Thus, some of HNFs_(mod) were not well controlled and behaved like normal or classic HNFs, resulting in weak diagonal diffraction peaks that also appeared at q_1 (red solid line in Fig. 3e, $\chi = 60^\circ$). It should be noted that the second peak at $\chi = 60^\circ$ was exceedingly strong compared to that for the case of OTS-modified AAO, and this resulted from the different molecular packing sequence, as shown in Fig. 4.

Now, in order to understand the in-layer modulation in the HNF_(mod) structure, previous studies of the columnar-to-smectic phase-transition model should be considered^{20,22}. Martinez-Perdiguero et al. explained this transition with a sliding model as follows. In the B1, columnar phase, bent-core molecules are

between neighbouring units. In the energetically favourable case, when the molecules have the same polar direction in the same layer plane, these cylinders can slightly slide to form pseudo-smectic modulated layers. Since this pseudo-smectic layer came from the adjacent discrete unit cell of the columnar phase, the B1 phase needs to be stabilised and the columnar building blocks in a layer should possess an identical polarisation direction. This sliding model can explain negligible differences in enthalpy between the columnar and smectic phases, and this condition is well-satisfied and fits with our system because AAO can be considered as a huge cold or hot reservoir because of the material characteristics and relative volume compared with LC materials.

Based on this model and our experimental results, the molecular arrangement and accompanying layered structures in HNFs_(mod) on the OTS- or PEG 6/9-treated AAO nanochannels can be described schematically in Fig. 4. On the LC-molecule-phobic surface (OTS), discrete cylindrical domains could freely slide to form transient layered structures with the same polar direction, resulting in the pseudo-layered structures like the B2 smectic phase that could smoothly transition into HNFs_(mod). In Fig. 4a and b, the model sketch shows how the layered structures were arranged on the LC-molecule-phobic surface based on the SEM and GIXD results, in which l_1 represents an interlayer d-spacing value of q_1 , and l_2 reflects an in-layer modulation value of q_2 . The tilted layer arrangement was derived from the diagonal patterns in GIXD (Fig. 3b) and the SEM image in Fig. 2d. In contrast, the LC-molecularphilic surface had a strong chemical affinity with the W618 molecules, and thus the cylindrical domains could perfectly slide but were held in the B1 configuration even after the temperature reached the range corresponding to the B4 phase. The layer spacing increased during the phase transition from B1 to B4 because tilted molecules in the layer stood up in the direction of the nanochannels. The crystallised layer structures

then formed modulated layers in the separated domains, as shown in Fig. 4c, d. The layer spacing¹⁰, was 44.21 Å, representing q_0 at $\chi = 0^\circ$; the layer undulation¹³, was 38.04 Å at $\chi = 32^\circ$ (white dashed line, tilted θ was $\sim 58^\circ$ in Fig. 4d) in Fig. 3e, d. Compared to the LC-molecule-phobic surface in Fig. 3b, diagonal patterns of the tilted layer arrangement in $\text{HNFs}_{(\text{mod})}$ (red line) were barely found but the major peak of the B4 phase on the PEG 6/9 surface was placed exactly at $\chi = 0^\circ$ (Fig. 3d). This was obtained from the result of the discontinuously packed columnar domains at intervals of half layer pitch (Figs. 2f and 4c). In addition, the 2D pattern in the wide-angle region supports this model, in which W618 has three rigid parts of aromatic rings and flexible alkyl tails (Fig. S3).

While the model of inter- and intralayer structures in the B4 phases at low temperature is clearly supported, the sequential structural changes during phase transition from the B1 phase to the B4 phase should be confirmed by an *in-situ* analytical system to support the hypothesis of our layer-formation process. This was carried out using *in-situ* GIXD of the structures ranging from isotropic to the B4 phase. All the data for NOBOW and W618 in this range of temperature are shown in Supplement information (Figs. S4 and S5). All conformational changes of NOBOW in the surface-modified nanochannels during the Iso-B2–B4 transition are similar to previous results¹⁶, indicating saddle-splay layer deformation at 138 °C in the B4 phase (fig. S4). In the case of W618, 2D patterns at 150 °C unexpectedly but clearly showed both radial peaks from a typical B1 mesophase lattice and a new centred peak from the layer structure in all the modified surfaces (Fig. S5). At 150 °C, q_{B1} (0.194 \AA^{-1}) was observed at $\chi = 0^\circ$, $\chi = 42^\circ$, and $\chi = 83^\circ$ (dashed line), which is the traditional peak of the B1 phase in the SiO_2 -coated nanochannel. As the sample was cooled to room temperature, the q_{B1} peaks were shifted to q_1 (0.132 \AA^{-1}) and changed their position to the diagonal direction, which means that the discrete columnar unit cells were gradually developing into a smectic layered structure. At 53 °C, only q_1 remained at $\chi = 60^\circ$, which corresponds to the traditional HNF pattern representing twisted layers¹⁶. Our analysis of optical images also supports the hypothesis that the columnar domains were simultaneously transformed to continuous smectic layered structures upon cooling (Fig. S6). Meanwhile, a centred peak of q_{B1} at $\chi = 0^\circ$ (0.288 \AA^{-1}) and 150 °C was still observed at 53 °C (0.293 \AA^{-1}), and the main layer peak of q_1 was deformed along the q_z axis in the PEG 6/9-modified nanochannel, as shown earlier (Figs. 3d, e and 4d). The hypothesis that the bamboo-like structure was derived from the B1 mesophase can be explained on the basis of the remaining q_{B1} at $\chi = 0^\circ$; the internal molecular conformation in the B1 mesophase could not be transformed to a layered structure affected by surface interaction.

Conclusions

In conclusion, we individually controlled and analysed the conformational change of $\text{HNFs}_{(\text{mod})}$ compared to classic HNFs using chemically treated AAO nanochannels. We obtained individual helical nanofilaments that, unlike those in the bulk state, maintained their straightness regardless of their helicity confined in porous alumina nanochannels. In addition, we observed that the molecules took on a particular orientation to the surface, forming the particular layer direction depending on their chemical affinity and the surface energy between the bent-

core molecules and the surface. As a result, helical nanofilaments and bamboo-like structures could be formed naturally and precisely, as shown by GIXD analysis of our system. Future attempts to combine the chemical and physical confinement effects will be helpful for better understanding of the fundamental studies on mesophases and hopefully lead to the development of basic design principles to obtain spontaneous LC-based materials with simple chemical treatments.

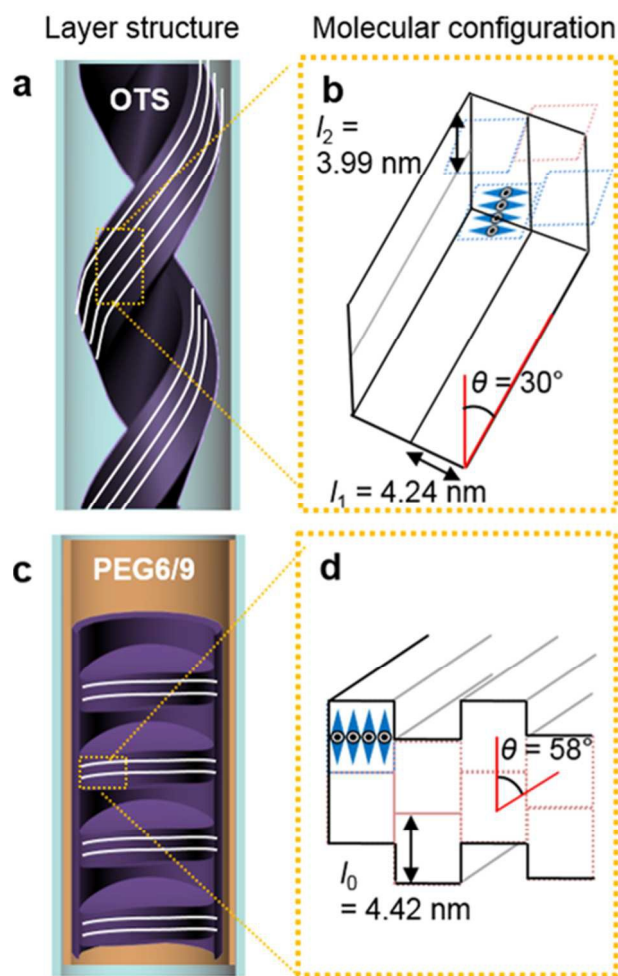


Figure 4. Schematic sketch of $\text{HNFs}_{(\text{mod})}$ and bamboo-like B4 structures from W618 in OTS- and PEG 6/9-treated AAO nanochannels. a, b, On the OTS-coated nanochannel surface, discrete rectangular columnar unit cells slid to form pseudo-layers²⁰ and finally formed $\text{HNF}_{(\text{mod})}$. c, d, On the PEG 6/9-coated surface, discrete rectangular columnar unit cells were held in the molecular-philic nanochannel wall and crystallized, maintaining their lattice upon cooling.

Experimental

Sample preparation. The bent-core molecules (NOBOW and W618) were prepared as previously reported^{3,12}. The homemade anodic aluminium-oxide nanochannel films were synthesised by a two-step anodization method²³ with high-purity annealed (99.99 %) aluminium foil from Alfa Aesar. The annealed foil

was electropolished in a mixture of perchloric acid and ethanol at low temperature in the constant-current mode. It was then anodised in 0.3 M oxalic acid at 10 °C under an applied voltage of 40 V for 7 h. After removing irregularly formed aluminium oxide in a mixture of chromic acid and phosphoric acid, the second anodisation under the same conditions was performed for 1 h. Following pore widening in a phosphoric acid solution at 38 °C for 20 min, highly uniform AAO nanochannels measuring 60 nm in diameter and 5 µm in length were obtained.

To chemically modify the walls of the AAO nanochannels effectively, silica coating via a sol-gel method was necessary. The silica coating in AAO has been previously reported^{14,15}. In brief, dried AAO was immersed in a SiCl₄ precursor and then rinsed with hexane, methanol, and ethanol. After drying in nitrogen gas, the AAO was heated to 120 °C over 1 h; this process was repeated three times. With this step, the inner wall of AAO and the surface of silicon wafer contain the same surface component (SiO₂), that is guaranteed to be identical for further surface modification. Each surface feature (Silanol-terminated AAO and SiO₂-containing silicon wafer were chemically modified with OTS (Gelest) and PEG 6/9 (90%, Gelest) as self-assembled monolayers¹³⁻¹⁵.

Bent-core LCs were simply loaded into the nanochannels by capillary force at the isotropic temperature. Upon cooling of the LC-loaded nanochannels at a cooling rate of 5 °C/min, mesogen in the 'test tube' became confined according to phase transition and finally, helical nanofilaments in the nanochannel complex were completed in the B4 phase. HNFs in the AAO thin film were bent and cross-sectioned vertically for SEM analysis of the internal structure.

GIXD analysis. All GIXD experiments were carried out at PLS-II (Pohang Accelerator Laboratory) in the Rep. of Korea. The samples were prepared with the same dimensions of 10 mm × 10 mm (in-plane area) × 180 µm (depth). The incidence X-ray beam was guided to the samples with an energy of 11.15 keV, a size of 70 µm (vertical) × 300 µm (horizontal), and a sample-to-detector distance (SDD) of 235 mm. To investigate the *in-situ* molecular orientation sequences, molecular cooling was conducted with a precisely controlled temperature gradient from 165 °C to 25 °C at a cooling rate of 5 °C/min. All diffraction patterns were acquired at every phase transition after 5 min of dwelling time to reach the thermal equilibrium state in each case. Before and after all GIXD experiments, morphological measurements were conducted to confirm the variations in the LC structure under different surface conditions.

Acknowledgements

The acknowledgements come at the end of an article after the conclusions and before the notes and references. This was supported by a grant from the National Research Foundation (NRF), funded by the Korean Government (2014M3C1A3052537, 2012M3A7B4049802 and 2014S1A2A2027911), and by the MRSEC Program funded by NSF DMR-1420736. Experiments at the PLS- II were supported in part by MSIP and POSTECH.

Notes and references

- ^a Graduate School of Nanoscience and Technology and KINC, KAIST, Daejeon, 305-701, Rep. of Korea
^b Pohang Accelerator Laboratory, POSTECH, Pohang, 790-784, Rep. of Korea
^c Department of Chemistry, Metropolitan State University of Denver, Denver, CO 80217, USA
^d Department of Chemistry and Biochemistry, University of Colorado, Boulder, CO 80309, USA
^e Department of Physics and Liquid Crystal Materials Research Center, University of Colorado, Boulder, CO 80309, USA
^f Department of Chemistry and Biochemistry, University of Maryland, College Park, MD 20742, USA

† These authors contributed equally to this work.

*To whom correspondence should be addressed.

Electronic Supplementary Information (ESI) available: [details of any supplementary information available should be included here]. See DOI: 10.1039/c000000x/

1. H. Takezoe, Y. Takanishi, *Jpn. J. Appl. Phys.* 2006, **45**, 597-625.
2. A. Zep, K. Sitkowska, D. Pocięcha and E. Gorecka, *J. Mater. Chem. C* 2014, **2**, 2323-2327. ea
3. L. E. Hough, H. T. Jung, D. Krüerke, M. S. Heberling, M. Nakata, C. D. Jones, D. Chen, D. R. Link, J. Zasadzinski, G. Heppke, J. P. Rabe, W. Stocker, E. Korblova, D. M. Walba, M. A. Glaser and N. A. Clark, *Science* 2009, **325**, 456-460.
4. H. Kim, Y. H. Kim, S. Lee, D. M. Walba, N. A. Clark, S. B. Lee and D. K. Yoon, *Liq. Cryst.* 2014, **41**, 328-341.
5. D. R. Link, D. M. Walba, *Science* 1997, **278**, 1924-1927.
6. D. A. Coleman, J. Fernsler, N. Chattham, M. Nakata, Y. Takanishi, E. Korblova, D. R. Link, R.-F. Shao, W. G. Jang, J. E. MacLennan, O. Mondainn-Monval, C. Boyer, W. Weissflog, G. Pelzl, L.-C. Chien, J. Zasadzinski, J. Watanabe, D. M. Walba, H. Takezoe and N. A. Clark, *Science* 2003, **301**, 1204-1211.
7. M. Nakata, D. R. Link, F. Araoka, J. Thisayukta, Y. Takanishi, K. Ishikawa, J. Watanabe and H. Takezoe, *Liq. Cryst.* 2001, **28**, 1301-1308.
8. F. Araoka, Y. N. Ha, Y. Kinoshita, B. Park, J. W. Wu and H. Takezoe, *Phys. Rev. Lett.* 2005, **94**, 137801.
9. J. Thisayukta, Y. Nakayama, S. Kawauchi, H. Takezoe and J. Watanabe, *J. Am. Chem. Soc.* 2000, **122**, 7441-7448.
10. D. Chen, J. E. MacLennan, R. Shao, D. K. Yoon, H. Wang, E. Korblova, D. M. Walba, M. A. Glaser and N. A. Clark, *J. Am. Chem. Soc.* 2011, **133**, 12656-12663.
11. D. K. Yoon, Y. Yi, Y. Shen, E. D. Korblova, D. M. Walba, I. Smalyukh and N. A. Clark, *Adv. Mater.* 2011, **23**, 1962-1967.
12. E. Tsai, J. M. Richardson, E. Korblova, M. Nakata, D. Chen, Y. Shen, R. Shao, N. A. Clark and D. M. Walba, *Angew. Chem. Int. Ed.* 2013, **125**, 5362-5365.
13. K. Y. Choi, J. J. Han, B. He and S. B. Lee, *J. Am. Chem. Soc.* 2008, **130**, 3920-3926.
14. K. Jayaraman, K. Okamoto, S. J. Son, C. Luckett, A. H. Gopalani, S. B. Lee and D. S. English, *J. Am. Chem. Soc.* 2005, **127**, 17385-17392.
15. A. Nan, X. Bai, S. J. Son, S. B. Lee and H. Ghandehari, *Nanolett* 2008, **8**, 2150-2154.

Journal Name

16. H. Kim, S. Lee, T. J. Shin, E. Korblova, D. M. Walba, N. A. Clark, S. B. Lee and D. K. Yoon, *Proc. Natl. Acad. Sci. U.S.A.*, 2014, **111**, 14342–14347.
17. C. Hong, T-T. Tang, C-Y. Hung, R-P.bPan and W. Fang, *Nanotechnol* 2010, **21**, 285201.
18. Y. Wu, G. Cheng, K. Katsov, S. W. Sides, J. Wang, J. Tang, G. H. Fredrickson, M. Moskovits and G. D. Stucky, *Nature* 2004, **3**, 816-822.
19. B. Platschek, A. Keilbach and T. Bein, *Adv. Mater.* 2011, **23**, 2395-2412.
20. J. Martinez-Perdiguero, J. Etxebarria, C. L. Folcia, J. Ortega, N. Gimeno and M. B. Ros, *Phys. Rev. E* 2010, **82**, 041706.
21. H. Kim, S. Lee, T. J. Shin, Y. J. Cha, E. Korblova, D. M. Walba, N. A. Clark, S. B. Lee and D. K. Yoon, *Soft Matter* 2013, **9**, 6185-6191.
22. C. L. Folcia, J. Etxebarria, J. Ortega and M. B. Ros, *Phys. Rev. E* 2006, **74**, 031702.
23. H. Masuda and K. Fukuda, *Science* 1995, **268**, 1466-1468.